NREL
NATIONAL RENEWABLE ENERGY LABORATORY

CdS/CdTe Solar Cells Containing Directly Deposited CdS_xTe_{1-x} Alloy Layers

Preprint

Joel N. Duenow, Ramesh G. Dhere,
Helio R. Moutinho, Bobby To, Joel W. Pankow,
Darius Kuciauskas, and Timothy A. Gessert

Presented at the 37th IEEE Photovoltaic Specialists Conference (PVSC 37)
Seattle, Washington
June 19-24, 2011

Conference Paper
NREL/CP-5200-50755
July 2011

Contract No. DE-AC36-08GO28308

NOTICE

Available electronically at http://www.osti.gov/bridge

Available for a processing fee to U.S. Department of Energy
and its contractors, in paper, from:

U.S. Department of Energy
Office of Scientific and Technical Information

P.O. Box 62
Oak Ridge, TN 37831-0062
phone: 865.576.8401
fax: 865.576.5728
email: mailto:reports@adonis.osti.gov

Available for sale to the public, in paper, from:

U.S. Department of Commerce
National Technical Information Service
5285 Port Royal Road
Springfield, VA 22161
phone: 800.553.6847
fax: 703.605.6900
email: orders@ntis.fedworld.gov
online ordering: http://www.ntis.gov/help/ordermethods.aspx

Cover Photos: (left to right) PIX 16416, PIX 17423, PIX 16560, PIX 17613, PIX 17436, PIX 17721

Printed on paper containing at least 50% wastepaper, including 10% post consumer waste.

CdS/CdTe SOLAR CELLS CONTAINING DIRECTLY DEPOSITED CdS_xTe_{1-x} ALLOY LAYERS

Joel N. Duenow, Ramesh G. Dhere, Helio R. Moutinho, Bobby To, Joel W. Pankow, Darius Kuciauskas, and Timothy A. Gessert
National Renewable Energy Laboratory, 1617 Cole Blvd., Golden, CO 80401

ABSTRACT

A CdS_xTe_{1-x} layer forms by interdiffusion of CdS and CdTe during the fabrication of thin-film CdTe photovoltaic (PV) devices. The CdS_xTe_{1-x} layer is thought to be important because it relieves strain at the CdS/CdTe interface that would otherwise exist due to the 10% lattice mismatch between these two materials. Our previous work [1] has indicated that the electrical junction is located in this interdiffused CdS_xTe_{1-x} region. Further understanding, however, is essential to predict the role of this CdS_xTe_{1-x} layer in the operation of CdS/CdTe devices. In this study, CdS_xTe_{1-x} alloy films were deposited by radio-frequency (RF) magnetron sputtering and co-evaporation from CdTe and CdS sources. Both RF-magnetron-sputtered and co-evaporated CdS_xTe_{1-x} films of lower S content ($x<0.3$) have a cubic zincblende (ZB) structure akin to CdTe, whereas those of higher S content have a hexagonal wurtzite (WZ) structure like that of CdS. Films become less preferentially oriented as a result of a $CdCl_2$ heat treatment (HT) at ~400°C for 5 min. Films sputtered in a 1% O_2/Ar ambient are amorphous as deposited, but show CdTe ZB, CdS WZ, and CdTe oxide phases after a $CdCl_2$ HT. Films sputtered in O_2 partial pressure have a much wider bandgap than expected. This may be explained by nanocrystalline size effects seen previously [2] for sputtered oxygenated CdS (CdS:O) films. Initial PV device results show that the introduction of a directly-deposited CdS_xTe_{1-x} alloy layer into the device structure produces devices of comparable performance to those without the alloy layer when a $CdCl_2$ HT is performed. Further investigation is required to determine whether the $CdCl_2$ heat treatment step can be altered or eliminated through direct deposition of the alloy layer.

INTRODUCTION

A CdS_xTe_{1-x} layer forms by interdiffusion of CdS and CdTe during the fabrication of thin-film CdTe PV devices in the standard superstrate configuration. High-temperature processing steps such as the close-spaced sublimation of CdTe and the post-deposition $CdCl_2$ HT contribute to formation of this alloy [1]. The CdS_xTe_{1-x} layer is thought to be important in fabricating high-performance CdTe devices because it relieves strain at the CdS/CdTe interface that would otherwise exist due to the large lattice mismatch (~10%) between these two materials. Our previous work indicated that the electrical junction is located in this interdiffused CdS_xTe_{1-x} region between a structurally compatible Te-rich n-type CdS_xTe_{1-x} alloy and p-type CdTe [1, 3].

The CdS_xTe_{1-x} alloy has been found to follow Vegard's law [4], such that lattice parameter values obtained from X-ray diffraction measurements can be used to calculate the mole fraction (x) for different phases of CdS_xTe_{1-x}. The bandgap (BG) of CdS_xTe_{1-x} has been described as a quadratic function of x [5], with values decreasing below the CdTe BG value of 1.5 eV, to as low as 1.41 eV at x~0.3, before increasing at higher x values. The alloy system also exhibits a miscibility gap (two-phase region) in which both a CdTe-rich zincblende (ZB) phase and CdS-rich wurtzite (WZ) phase may be present simultaneously at equilibrium. The composition of each phase in the two-phase region is the same as in the corresponding single-phase regions at the edges of the miscibility gap, with the relative quantity of each phase present varying with x [6]. Single-phase films, however, have been grown within the miscibility gap, implying non-equilibrium growth methods were used. The phases generally separated after a $CdCl_2$ HT [6-8]. We found similar behavior in this study.

Further understanding of CdS_xTe_{1-x} alloys is essential to predict the role of the CdS_xTe_{1-x} layer in the operation of CdS/CdTe devices. In this study, we investigate this alloy layer by depositing CdS_xTe_{1-x} films using two methods. We also present preliminary results in which the alloy layer has been implemented in PV devices.

EXPERIMENTAL DETAILS

We deposited CdS_xTe_{1-x} films by radio-frequency (RF) magnetron sputtering using targets of three compositions: 10/90, 25/75, and 60/40 wt.% CdS/CdTe. Films were deposited at room temperature (RT; no intentional heating) and at 300°C. Because little difference was seen between films grown at RT and at 300°C, only the 300°C results are presented here. In addition, two deposition ambients were used—100% Ar and 1% O_2/Ar. The ratio was measured using an ion gauge. Films were also deposited by co-evaporation from CdTe and CdS sources using Radak II effusion cells. The geometry of the co-evaporation system enabled us to obtain a range of compositions during a single deposition. The films were deposited onto three different substrates—Corning 7059 glass, Corning 7059 glass/450-nm SnO_2:F/150-nm SnO_2, and Corning 7059 glass/SnO_2:F/SnO_2/125-nm sputtered CdS:O—to be amenable to the different types of characterization performed on the films. Reflectance and transmittance measurements were performed using a Cary 6000i UV-Vis-NIR spectrophotometer. Electron-probe microanalysis (EPMA) was performed using a beam energy of 5 kV to obtain film composition. X-ray diffraction

(XRD; Rigaku Ultima IV) θ-2θ measurements were performed using Cu K_α radiation to examine the structure of the CdS_xTe_{1-x} films. Electron backscatter diffraction (EBSD; FEI FEG SEM Nova 630 NanoSEM with an EDAX Pegasus/Hikari A40 EDS/EBSD system) measurements were performed to examine grain orientation and size for selected films. PV devices were grown using the following structure: Corning 7059 glass / 450 nm SnO_2:F by chemical vapor deposition (CVD) / 400 nm SnO_2 by CVD / 80-125 nm CdS / 300 nm CdS_xTe_{1-x} / 3 μm CdTe by evaporation at 400°C / 500 nm sputtered ZnTe:Cu (containing 2 wt.% Cu) at 300°C / 500 nm sputtered Ti.

RESULTS AND DISCUSSION

Composition of the ~150-nm-thick sputtered CdS_xTe_{1-x} alloy films was measured using EPMA (Figure 1). Films were grown in 100% Ar and 1% O_2/Ar both before and after a 5-min vapor $CdCl_2$ HT at 400°C. Films grown from the 10/90 wt.% CdS/CdTe target show little compositional change between the different deposition ambients and after the $CdCl_2$ HT. Films grown from the 25/75 and 60/40 wt.% CdS/CdTe targets in the 100% Ar ambient display a slight enrichment in S (or, equivalently, a loss of Te) after the $CdCl_2$ HT. All films appear S-deficient, however, compared to the manufacturer's stated target composition. This may be due to differences in sticking coefficient on the substrate of the S and Te species. Two ~300-nm-thick evaporated CdS_xTe_{1-x} films (Figure 2) were deposited using different combinations of CdS and CdTe effusion cell temperatures. The as-deposited films (solid lines) show the expected gradient in x across the substrate. The evaporated films also show a significant relative enhancement in S (or loss of Te) after the $CdCl_2$ HT.

CdS_xTe_{1-x} alloy film structure was investigated using XRD. Figure 3 shows θ-2θ scans of films grown from the 10/90 wt.% CdS/CdTe target in the 100% Ar and 1% O_2/Ar ambients both before and after a $CdCl_2$ HT. Films examined using XRD were deposited on Corning 7059 glass/450-nm SnO_2:F/150-nm SnO_2/125-nm sputtered CdS:O substrates similar to those used for CdTe PV devices. Tetragonal SnO_2, cubic ZB CdTe, and hexagonal WZ CdS peaks are indicated. The as-deposited film grown in 100% Ar shows one prominent peak, CdTe ZB (111). Other peaks in this spectrum are due to the SnO_2 films on the substrate. After a $CdCl_2$ HT is performed on this film, the CdTe ZB (111) peak decreases in intensity, while small CdTe ZB (220) and (311) peaks, and CdS WZ (100), (002), and (101) peaks, appear. This behavior indicates a decrease in preferential orientation after the $CdCl_2$ HT. The film grown in 1% O_2/Ar is amorphous as deposited. After the $CdCl_2$ HT, however, many CdTe ZB and CdS WZ phases appear, in addition to prominent CdTe oxide phases (e.g., $CdTeO_3$, $CdTe_2O_5$). Further work is required to identify which oxide phases are dominant. A summary of XRD results for the sputtered films is shown in Table 1. Films grown in 100% Ar from the 60/40 wt.% CdS/CdTe target contain only CdS WZ phases, both before and after the $CdCl_2$ HT, whereas films of higher CdTe content in this ambient show both CdTe ZB and CdS WZ phases. All films grown in 1% O_2/Ar are amorphous as deposited. The CdTe oxide peaks observed after the $CdCl_2$ HT are much less intense for the 25/75 and 60/40 wt.% CdS/CdTe films than for the 10/90 wt.% film.

XRD measurements were also performed on evaporated CdS_xTe_{1-x} alloy films both before and after a $CdCl_2$ HT at 390°C. Measurements were performed at several points on the film because of the composition gradient. The CdTe ZB (111) peak was observed to shift to an intermediate position between it and the adjacent CdS WZ (100) peak as the S content increased. After the $CdCl_2$ HT, the CdTe ZB (111) peak shifts toward its expected position, while other CdTe ZB and CdS WZ phases appear, indicating a decrease in film preferential orientation. These data are summarized in Table 2. The separation of the CdTe ZB(111) and CdS WZ (100) peaks suggests that phase separation occurs as a result of the $CdCl_2$ HT.

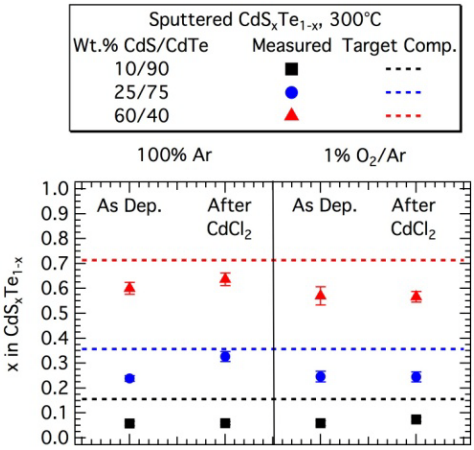

Figure 1 Measured x values (obtained using EPMA) for sputtered CdS_xTe_{1-x} films. Dashed lines indicate the manufacturer's stated target composition.

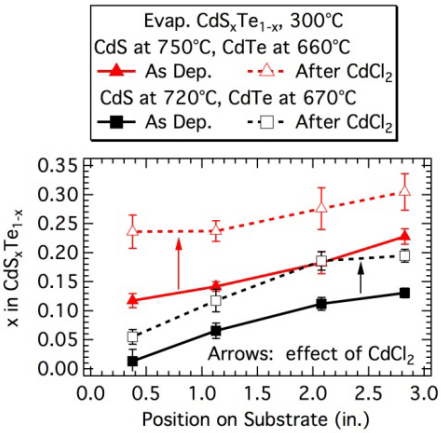

Figure 2 Measured x values (obtained using EPMA) for evaporated CdS_xTe_{1-x} films. Evaporated films were measured at four positions because of the inherent composition gradient across the substrate due to the deposition system geometry.

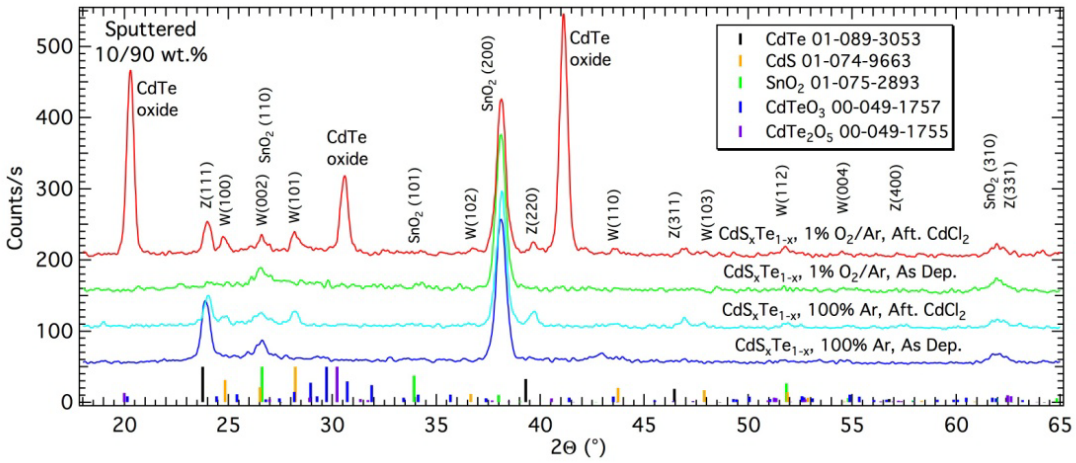

Figure 3 XRD scans for sputtered CdS_xTe_{1-x} films grown from the 10/90 wt.% CdS/CdTe target. Growth ambient and post-deposition treatment are shown on the plot. Peak positions from the powder diffraction files corresponding to these materials are shown at the bottom (with corresponding file numbers shown in the upper right).

Wt.% CdS/CdTe	100% Ar		1% O_2/Ar	
	As Deposited	After $CdCl_2$	As Deposited	After $CdCl_2$
10/90	CdTe ZB	CdTe ZB CdS WZ	Amorphous	CdTe ZB CdS WZ Strong oxide phases
25/75	CdTe ZB Minor CdS WZ	CdTe ZB CdS WZ	Amorphous	CdTe ZB CdS WZ Oxide phases
60/40	CdS WZ	CdS WZ	Amorphous	CdS WZ Oxide phases

Table 1 Phases present in sputtered CdS_xTe_{1-x} films grown in 100% Ar and 1% O_2/Ar before and after a $CdCl_2$ HT.

CdS Content	As Deposited	After $CdCl_2$
Lower (x = 0.01 to 0.12 as deposited)	CdTe ZB (111)	CdTe ZB Minor CdS WZ
Higher (x = 0.12 to 0.23 as deposited)	CdTe ZB (111), shifted toward CdS WZ (100) at high S	CdTe ZB CdS WZ

Table 2 Phases present in evaporated CdS_xTe_{1-x} films before and after a $CdCl_2$ HT.

Analysis was performed to extract the lattice constants and mole fraction of the CdTe ZB phase from the XRD data. The lattice constant a_{Cubic} was determined using $a_{Cubic} = d\sqrt{h^2 + k^2 + l^2}$, where $d = \lambda_a / (2\sin\theta)$ is calculated from the measured 2θ peak position, λ_α = 1.540562 Å is the wavelength of the Cu K_α radiation, and h, k, and l are the Miller indices for the diffraction peak. When multiple CdTe ZB peaks were present, the a_{Cubic} values were plotted as a function of the Nelson-Riley-Sinclair-Taylor (NRST) function [6],

$$NRST = \frac{1}{2}\left(\frac{\cos^2\theta}{\sin\theta} + \frac{\cos^2\theta}{\theta}\right).$$

Fitting a line to these points enabled a lattice constant of greater precision to be found by extrapolating to normal incidence at $NRST$ = 0 [6]. Vegard's law, which applies to the CdTe-CdS alloy system [4], was then used to determine the mole fraction, x, for the cubic ZB phase:

$$x = \frac{a_{CdS_xTe_{1-x}(Cubic)} - a_{CdTe}}{a_{CdS} - a_{CdTe}}.$$

For cubic phases, a_{CdTe} = 6.481 Å and a_{CdS} = 5.818 Å.

Figure 4 compares the x values obtained from EPMA and XRD for CdS_xTe_{1-x} alloy films sputtered in 100% Ar and subjected to a $CdCl_2$ HT. EPMA values measure the composition of the whole film. At higher S contents, EPMA values strongly exceed those obtained using the XRD analysis of the CdTe cubic ZB peaks, which measures the composition of the ZB phase only. The difference indicates that the film composition is within the CdS/CdTe miscibility

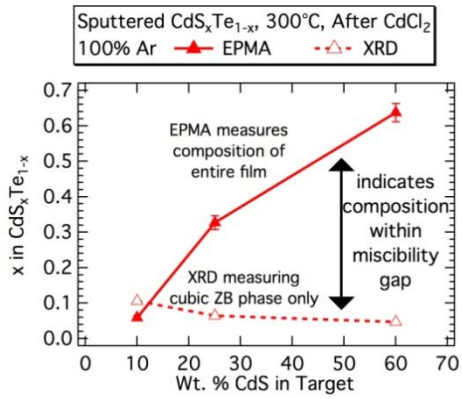

Figure 4 Mole fraction (x) obtained from EPMA and XRD measurements for sputtered CdS_xTe_{1-x} films.

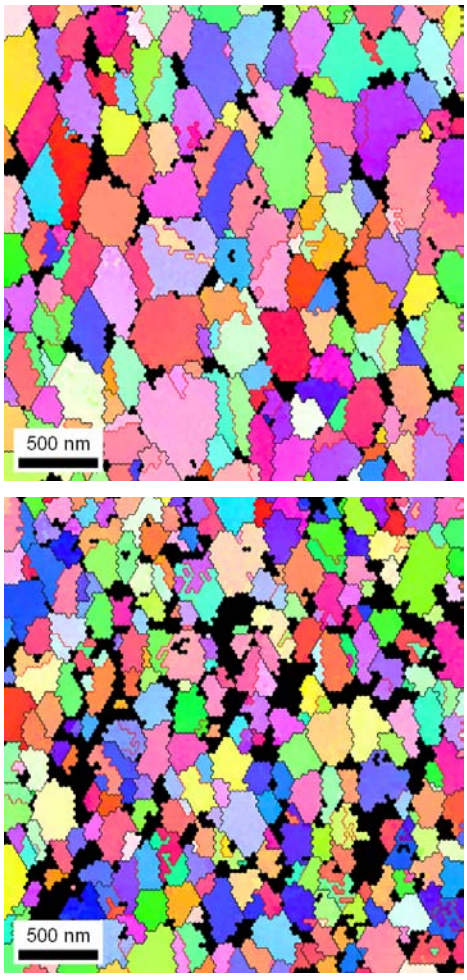

Figure 5 EBSD images for a sputtered film (upper panel; x = 0.059, grain size 360 nm) and an evaporated film (lower panel; x = 0.28, grain size 240 nm). Black lines indicate grain boundaries; red lines indicate $\sum 3$ twin boundaries. Both films were imaged after a $CdCl_2$ HT.

gap for films of the higher two S contents. The miscibility gap was measured to lie between x = 0.058 and x = 0.97 [7] at temperatures of 415°C. Mole fraction valuesmeasured by XRD for the Te-rich cubic ZB phase in this study are consistent with the x = 0.058 observed by Jensen *et al.* [7]. Similar x values were observed for the evaporated films also (not shown).

To obtain information about grain orientation and size in these films, EBSD measurements were performed (Figure 5) on CdS_xTe_{1-x} alloy films grown on Corning 7059/SnO_2:F/SnO_2/CdS:O substrates. One sputtered film and one evaporated film were measured after a $CdCl_2$ HT and a 0.5%-concentrated bromine-methanol etch for 2 s. Grains of both films are randomly oriented, indicated by the different colors of each grain. Pole figures (not shown) confirm this random orientation. The grain size of the sputtered film is 360 nm, whereas that of the evaporated film is 240 nm. This difference may be due to the greater adatom surface energy of the sputtering process. The $CdCl_2$ HT temperature for the sputtered film was also 10°C higher (400°C vs. 390°C), which may have contributed to increased recrystallization.

The BG of sputtered and evaporated CdS_xTe_{1-x} films was calculated by measuring the reflectance and transmittance, calculating the absorption coefficient (α) [9], and plotting $(\alpha h\nu)^2$ vs. $h\nu$, where $h\nu$ is the photon energy. The evaporated films appear to have similar BG values (Figure 6), indicating that these films have phase separated due to the miscibility gap. The sputtered films deposited in the 100% Ar ambient also appear to have values near the 1.5 eV BG of CdTe. An interesting phenomenon was observed for the films deposited in the

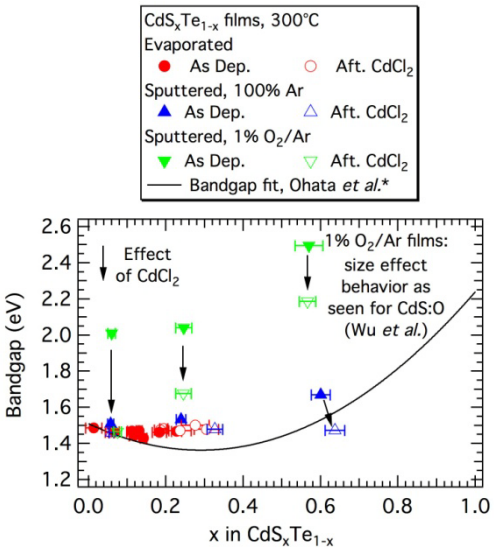

Figure 6 Bandgap vs. mole fraction (x) for sputtered and evaporated CdS_xTe_{1-x} films. The black curve was determined by Ohata et al. [5] by fitting experimental data.

1% O_2/Ar ambient. As deposited, these films had BG values much higher than expected. In fact, the 60/40 wt.% CdS/CdTe film had a BG value higher than that of CdS itself. We suspect this behavior is similar to that observed for CdS:O by Wu *et al.* [2], in which CdS films were sputtered in O_2 partial pressure. In that study, amorphous CdS:O films with BGs of up to 3.1 eV were deposited. The increase in BG was attributed to nanocrystalline quantum size effect behavior. We believe a similar effect is occurring in CdS_xTe_{1-x} films deposited in O_2 partial pressure. After a $CdCl_2$ HT, the low-S film decreases to a BG near that of CdTe, whereas the higher-S films decrease in BG substantially, but not to the expected levels. This decrease is consistent with partial grain recrystallization and growth occurring as a result of the HT, although it seems to be incomplete.

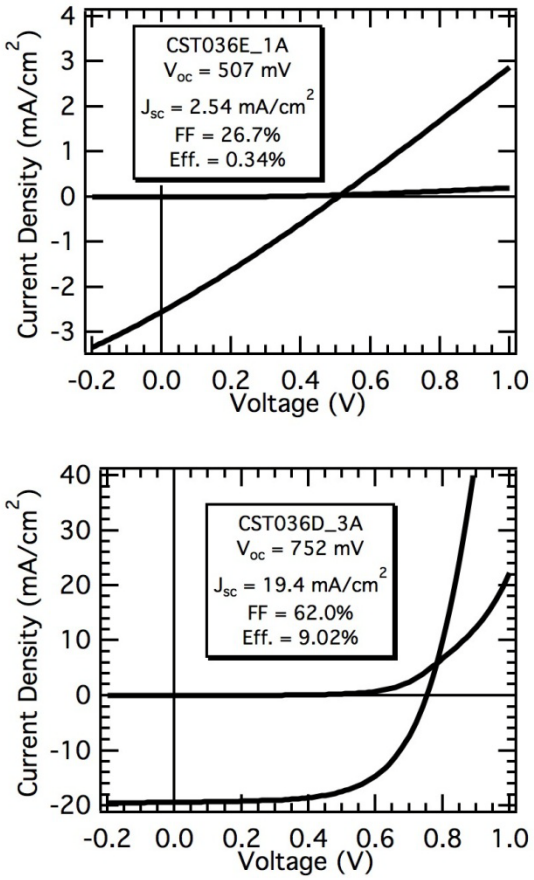

Figure 7 PV devices incorporating a 300-nm-thick sputtered CdS_xTe_{1-x} layer deposited from a target of composition 25/75 wt.% CdS/CdTe (leading to measured x = 0.24). Open-circuit voltage (V_{oc}), short-circuit current (J_{sc}), fill factor (FF), and efficiency (Eff.) are shown on the plot. The device in the top panel received no $CdCl_2$ HT, while that in the bottom panel was treated at 405°C for 5 min.

Preliminary device work was performed using a CdS_xTe_{1-x} alloy layer deposited either by sputtering or co-evaporation. For devices utilizing a sputtered alloy layer, the film was deposited onto a window layer of 125 nm of sputtered CdS:O. The deposition of 3-5 μm of CdTe by evaporation onto substrates heated to 400°C followed. Devices that received no $CdCl_2$ HT after the CdTe deposition all showed poor performance (Figure 7, top panel), despite having a pre-formed alloy region. A higher CdTe deposition temperature may be required to form a p-type CdTe absorber layer. In future work, we will use the close-spaced sublimation technique to deposit CdTe at higher temperatures (450-500°C) to investigate this possibility. In previous work, it was found that only slight CdS/CdTe interdiffusion occurred during CdTe deposition in this temperature range [3]. Depositing CdTe at these temperatures, therefore, is not expected to adversely affect study of the directly-deposited alloy layer in these devices. Devices containing the alloy layer that were subjected to a $CdCl_2$ HT after the CdTe deposition (Figure 7, lower panel) showed performance comparable to that of baseline devices with no alloy layer. A baseline device had the following parameters: V_{oc} = 763 mV, J_{sc} = 20.2 mA/cm^2, FF = 59.7%, and eff. = 9.19%. The comparable performance of devices containing the alloy layer shows that introduction of this directly-deposited layer is not fundamentally detrimental to device performance. In future work, we will further investigate the effects of the $CdCl_2$ HT on the directly-deposited alloy layer in PV devices, as the $CdCl_2$ HT is known to enhance interdiffusion of CdS and CdTe in standard devices.

Devices were also fabricated using a CdS_xTe_{1-x} alloy layer deposited by co-evaporation of CdS and CdTe at a substrate temperature of 400°C. The mole fraction of the alloy film was ≈x 0.07. This layer was followed by deposition of a 3-5 μm CdTe film at 400°C without breaking vacuum. The devices that received no $CdCl_2$ HT performed poorly (not shown), similar to the device seen in the top panel of Figure 7. After a $CdCl_2$ HT at 405°C, devices utilizing ≈100 nm of chemical-bath deposited (CBD) CdS (Figure 8, top panel) showed performance comparable to baseline devices without the alloy layer (baseline device parameters: V_{oc} = 740 mV, J_{sc} = 22.6 mA/cm^2, FF = 66.0%, eff. = 11.0%). The device utilizing 80 nm of sputtered CdS:O (Figure 8, lower panel), however, showed lower performance than that of the CBD CdS device and the sputtered CdS:O baseline. Further optimization work will be performed to enhance the performance of devices utilizing a sputtered CdS:O window layer.

CONCLUSIONS

CdS_xTe_{1-x} alloy films were deposited by RF magnetron sputtering and co-evaporation. As-deposited sputtered films grown in 100% Ar from targets containing 10/90 and 25/75 wt.% CdS/CdTe have a cubic CdTe ZB structure, whereas those grown from a target of 60/40 wt.% CdS/CdTe have a hexagonal CdS WZ structure. Films

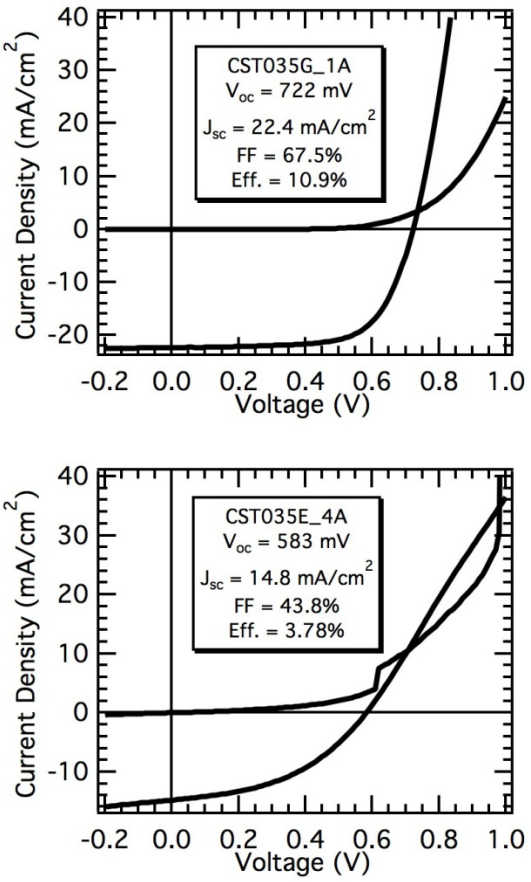

Figure 8 PV devices incorporating a 300-nm-thick evaporated CdS_xTe_{1-x} alloy layer of x ≈ 0.07. The device in the top panel contains a window layer of ≈100 nm of CBD CdS, while the device in the bottom panel contains 80 nm of sputtered CdS:O.

become less preferentially oriented as a result of a vapor $CdCl_2$ HT at 400°C for 5 min. Films sputtered in a 1%O_2/Ar ambient are amorphous as deposited, but show CdTe ZB, CdS WZ, and CdTe oxide phases after a $CdCl_2$ HT. Evaporated films primarily consist of the CdTe ZB phase as deposited, but the CdTe ZB (111) peak is shifted significantly toward the adjacent CdS WZ (100) peak for films of higher S content. These two peaks become distinct after a $CdCl_2$ HT, indicating phase separation has occurred. Both sputtered and evaporated films have randomly oriented grains after a $CdCl_2$ HT. The grain size of the sputtered film is larger than that of the evaporated film (360 vs. 240 nm). CdS_xTe_{1-x} alloy films sputtered in 1% O_2/Ar are amorphous as deposited and have a much higher bandgap than expected. This may be explained by nanocrystalline size effects seen previously [2] for CdS:O films. PV devices were fabricated using a directly-deposited CdS_xTe_{1-x} alloy film between the CdS and CdTe layers. Despite the presence of a pre-formed alloy layer, devices that received no $CdCl_2$ treatment performed poorly. Higher CdTe deposition temperatures that may enable higher performance by ensuring p-type CdTe will be investigated. Devices containing the alloy layer that received a $CdCl_2$ HT after the CdTe deposition in many cases showed comparable performance to baseline devices without the alloy layer, suggesting that this directly-deposited alloy layer is not fundamentally detrimental to device performance.

Future work will include additional EBSD measurements to identify CdS_xTe_{1-x} phases and their intermixing both before and after a $CdCl_2$ HT. Auger electron spectroscopy and X-ray photoelectron spectroscopy will be used to examine the CdTe oxides that result from the $CdCl_2$ HT of films grown in 1% O_2/Ar. In future PV device work, we first plan to replicate the existing superstrate device structure using directly deposited CdS_xTe_{1-x} layers in PV devices. We also expect to design and deposit new superstrate and substrate PV device structures using these directly deposited layers.

ACKNOWLEDGEMENTS

This work was supported under DOE Contract No. DE-AC36-08-G028308 to NREL.

REFERENCES

[1] R. G. Dhere, Y. Zhang, M. J. Romero, S. E. Asher, M. Young, B. To, R. Noufi, and T. A. Gessert, "Investigation of Junction Properties of CdS/CdTe Solar Cells and Their Correlation to Device Properties," *Proc. of the 33rd Photovoltaic Specialists Conference*, San Diego, CA: IEEE, 2008.

[2] X. Wu, Y. Yan, R. G. Dhere, Y. Zhang, J. Zhou, C. Perkins, and B. To, "Nanostructured CdS:O Film: Preparation, Properties, and Application," *phys. stat. sol. (c)* **1**, 2004, pp. 1062-1066.

[3] R. G. Dhere, "Study of the CdS/CdTe Interface and Its Relevance to Solar Cell Properties," Ph.D. Thesis, University of Colorado, 1997.

[4] K. Ohata, J. Saraie, and T. Tanaka, "Phase Diagram of the CdS-CdTe Pseudobinary System," *Japan. J. Appl. Phys.* **12**, 1973, pp. 1198-1204.

[5] K. Ohata, J. Saraie, and T. Tanaka, "Optical Energy Gap of the Mixed Crystal CdS_xTe_{1-x}," *Japan. J. Appl. Phys.* **12**, 1973, pp. 1641-1642.

[6] D. G. Jensen, "Alloys in Cadmium Telluride Solar Cells," Ph.D. Thesis, Stanford University, 1997.

[7] D. G. Jensen, B. E. McCandless, and R. W. Birkmire, "Thin Film Cadmium Telluride-Cadmium Sulfide Alloys and Devices," *Proc. of the 25th Photovoltaic Specialists Conference*, Washington, D.C.: IEEE, 1996.

[8] B. E. McCandless, G. M. Hanket, D. G. Jensen, and R. W. Birkmire, "Phase Behavior in the CdTe-CdS Pseudobinary System," *J. Vac. Sci. Technol. A* **20**, 2002, pp. 1462-1467.

[9] J. I. Pankove, *Optical Processes in Semiconductors*. New York, NY: Dover Publications, Inc., 1971.